Optimization of Surface Configuration in IRS-Aided MIMO-VLC: A BER Minimization Approach

Xin Zhong, Chen Chen, *Senior Member, IEEE*, Wanli Wen, *Member, IEEE*, Min Liu, H. Y. Fu, *Senior Member, IEEE*, and Harald Haas, *Fellow, IEEE*

***Abstract*—Due to its ability to reconfigure the optical channel, intelligent reflecting surface (IRS) has revealed its great potential for enhancing the performance of visible light communication (VLC) systems. In this paper, we apply a mirror array-based IRS in typical multiple-input multiple-output based VLC (MIMO-VLC) systems and optimize the IRS configuration to minimize the system bit error rate (BER). By utilizing the tight analytical BER upper bound, a BER minimization problem is formulated subject to the IRS configuration constraints. To solve this problem, an optimization algorithm is proposed which decomposes the original problem into three sub-problems, and the complexity of the algorithm is analyzed. The superiority of the obtained optimal IRS configuration scheme over the baseline scheme in terms of BER performance has been successfully verified through simulations in an indoor IRS-aided 4×4 MIMO-VLC system applying different MIMO techniques.**

***Index Terms*—Intelligent reflecting surface, multiple-input multiple-output, visible light communication.**

I. Introduction

VISIBLE light communication (VLC) has been widely envisioned as a key enabling technology for the sixth-generation (6G) wireless communication systems, owing to its inherent advantages such as abundant and license-free spectrum, no electromagnetic interference radiation, low-cost front-ends and high physical-layer security [1], [2]. Particularly, by re-using the illumination light-emitting diodes (LEDs), VLC can fulfill the dual-function of communication and illumination in typical indoor environments [3]. To provide efficient and uniform illumination for an indoor area, multiple LEDs are usually mounted on the ceiling, which naturally enable multiple-input multiple-output (MIMO) transmission in VLC systems [4]. As a result, MIMO-based VLC (MIMO-VLC) has been attracting ever-increasing research interests in recent years. So far, three MIMO transmission techniques, including repetition coding (RC), spatial modulation (SM), and spatial multiplexing (SMP), have been widely considered in most of the MIMO-VLC systems [5], [6], [7], [8], [9]. Moreover, advanced MIMO transmission techniques such as user-centric MIMO and generalized optical MIMO techniques have been further proposed for substantial performance improvement of MIMO-VLC systems [10], [11], [12].

Although MIMO transmission reveals potential for enhancing the performance of VLC, the performance gain of MIMO transmission in practical VLC systems is still greatly limited, which is mainly due to the high channel correlation caused by the small receiver separation [6]. To overcome the high channel correlation issue in MIMO-VLC systems, several techniques have already been reported in the literature. For example, imaging receiver has been adopted to de-correlate the multiplexed channels for MIMO-VLC systems in [13], [14], [15], angle diversity transmitter and angle diversity receiver have been introduced to mitigate channel correlation in MIMO-VLC systems in [16], [17], [18], and various precoding and equalization techniques via digital signal processing have also been applied to reduce the high channel correlation in MIMO-VLC systems [19], [20], [21]. Nevertheless, all the above-mentioned techniques address the high channel correlation issue by adjusting the hardware or software parts of the transceivers, which might be challenging in practical MIMO-VLC systems due to the limited transceiver resources.

Lately, intelligent reflecting surface (IRS) has been proposed to efficiently enable a smart and reconfigurable environment for wireless networks [22]. Due to its ability to reconfigure and modify the optical channel, IRS has also been attracting increasing attention for its application in VLC systems [23], [24]. For example, the optical channel of IRS-based VLC systems has been characterized in [25], [26], the resource management of IRS-aided VLC systems has been considered in [27], [28], and IRS has been further applied to enhance the security of VLC systems in [29], [30]. Most recently, IRS has also been introduced for performance improvement in MIMO-VLC systems [31], [32], [33]. The utilization of IRS in MIMO-VLC systems can efficiently modify the optical MIMO channels and the performance of MIMO-VLC systems can be substantially improved by properly configuring the IRS surface. Hence, the surface configuration of IRS plays an important role in IRS-aided MIMO-VLC systems and it is of practical significance to

Manuscript received 29 November 2023; revised 25 April 2024; accepted 29 April 2024. Date of publication 1 May 2024; date of current version 9 May 2024. This work was supported in part by the National Natural Science Foundation of China under Grant 62271091 and in part by the Natural Science Foundation of Chongqing under Grant cstc2021jcyj-msxmX0480. *(Corresponding authors: Chen Chen; Wanli Wen.)*

Xin Zhong, Chen Chen, Wanli Wen, and Min Liu are with the School of Microelectronics and Communication Engineering, Chongqing University, Chongqing 400044, China (e-mail: 201912131098@cqu.edu.cn; c.chen@cqu.edu.cn; wanli_wen@cqu.edu.cn; liumin@cqu.edu.cn).

H. Y. Fu is with Tsinghua Shenzhen International Graduate School, Tsinghua University, Shenzhen 518055, China (e-mail: hyfu@sz.tsinghua.edu.cn).

Harald Haas is with the Technology Innovation Centre, Department of Electronic and Electrical Engineering, University of Strathclyde, G1 1RD Glasgow, U.K. (e-mail: harald.haas@strath.ac.uk).

Digital Object Identifier 10.1109/JPHOT.2024.3395894

obtain an optimal surface configuration for a given IRS-aided MIMO-VLC system. In [31], the surface configuration of IRS in MIMO-VLC systems has been optimized by maximizing the asymptotic capacity. In [32], the IRS configuration and the transmitter emission power have been jointly optimized by maximizing the system capacity. In [33], the IRS configuration and transceiver signal processing have been jointly designed to minimize the mean square error (MSE) of the IRS-aided MIMO-VLC systems. Moreover, the IRS configuration has also been optimized to minimize the outage probability of various VLC systems [34], [35].

In the real implementation of IRS-aided MIMO-VLC systems, bit error rate (BER) is usually a more practical performance metric which determines the actual transmission performance of the MIMO links [6]. Nevertheless, the state-of-the-art designs of IRS configuration only aim to maximize the capacity or minimize the MSE of MIMO-VLC systems, while the IRS configuration which minimizes the BER of MIMO-VLC systems has not yet been considered. Moreover, the current works only have investigated one specific MIMO transmission technique, i.e., SMP, in the IRS-aided MIMO-VLC systems, while other popular MIMO transmission techniques such as RC and SM have all been neglected. In order to show the feasibility of applying IRS in a general MIMO-VLC system, it is necessary to take all these popular MIMO transmission techniques into consideration.

To investigate the practical use of IRS in a general MIMO-VLC system, in this paper, we propose to optimize the IRS configuration by minimizing the BER of MIMO-VLC systems. The main contributions of this work can be summarized as follows:

- Proposal of IRS configuration optimization by minimizing the BER of a general MIMO-VLC system, where three popular MIMO transmission techniques including RC, SM and SMP are considered.
- Formulating the optimization problem to minimize the BER of the IRS-aided MIMO-VLC system by utilizing the tight analytical error bound.
- Solving the optimization problem by decomposing the original NP-hard problem into three solvable subproblems, and further analyzing the complexity of the proposed optimization algorithm.
- Validating the feasibility and superiority in terms of BER performance of the obtained optimal IRS configuration in a typical indoor 4×4 MIMO-VLC system considering different MIMO transmission techniques, PD positions and IRS sizes by using the MATLAB software.

The remainder of this paper is structured as follows. In Section II, the mathematical model of IRS-aided MIMO-VLC systems in a typical indoor environment is first described. In Section IV, the optimization of IRS configuration in IRS-aided MIMO-VLC systems is provided. Simulation results and discussions are presented in Section IV. Finally, Section V concludes the paper.

II. System Model

In this section, we describe the mathematical model of IRS-aided MIMO-VLC systems in a typical indoor environment. Fig. 1(a) illustrates the model of an IRS-aided MIMO-VLC system equipped with N_t LEDs and N_r photodetectors (PDs), where the LED array is mounted on the ceiling and the PD array is located over the receiving plane. Assuming $\mathbf{x} = (x_1, x_2, \ldots, x_{N_t})^T$ denote the transmitted signal vector, the received signal vector $\mathbf{y} = (y_1, y_2, \ldots, y_{N_r})^T$ can be expressed by

$$\mathbf{y} = \mathbf{H}\mathbf{x} + \mathbf{n}, \tag{1}$$

where $\mathbf{H} \in \mathbb{R}_+^{N_r \times N_t}$ represents the $N_r \times N_t$ MIMO channel matrix and $\mathbf{n} = (n_1, n_2, \ldots, n_{N_r})^T$ denotes the additive white Gaussian noise (AWGN) vector. More specifically, $\mathbf{H}$ can be given by

$$\mathbf{H} = \begin{pmatrix} h_{1,1} & \cdots & h_{1,N_t} \\ \vdots & \ddots & \vdots \\ h_{N_r,1} & \cdots & h_{N_r,N_t} \end{pmatrix}, \tag{2}$$

where $h_{r,t}$ $(r = 1, 2, \ldots, N_r; t = 1, 2, \ldots, N_t)$ denotes the channel gain between the r-th PD and the t-th LED.

A. Channel Model

In a typical IRS-aided MIMO-VLC system, as illustrated in Fig. 1(a), the channel matrix $\mathbf{H}$ consists of three main components: the LOS component $\mathbf{H}_{\text{LOS}}$, the diffuse NLOS component $\mathbf{H}_{\text{NLOS}}$ and the IRS component $\mathbf{H}_{\text{IRS}}$. Hence, $\mathbf{H}$ can be rewritten as

$$\mathbf{H} = \mathbf{H}_{\text{LOS}} + \mathbf{H}_{\text{NLOS}} + \mathbf{H}_{\text{IRS}}. \tag{3}$$

For simplicity and without loss of generality, we assume the IRS-aided MIMO-VLC system has a flat frequency response, and the PDs are vertically oriented towards the ceiling. Hence, the calculation of the channel gains in each component can be introduced as follows.

1) LOS Channel Gain: Assuming the LEDs follow a Lambertian emission pattern, as can be seen from Fig. 1(a), the LOS channel gain between the r-th PD and the t-th LED can be calculated by [3]

$$h_{r,t}^{\text{LOS}} = \frac{(l+1)\rho A}{2\pi d_{r,t}^2} \cos^l(\varphi_{r,t}) T_s g(\theta_{r,t}) \cos(\theta_{r,t}) \times \text{rect}\left(\varphi_{r,t}, \theta_{r,t}, \Psi, \Phi\right), \tag{4}$$

where $l = -\ln 2 / \ln(\cos(\Psi))$ denotes the Lambertian emission order with Ψ being the semi-angle at half power of the LEDs; ρ and A are the responsivity and the active area of the PDs, respectively; $d_{r,t}$ is the transmission distance between the r-th PD and the t-th LED; $\varphi_{r,t}$ and $\theta_{r,t}$ are the emission angle and the incident angle from the t-th LED to the r-th PD, respectively; T_s is the gain of the optical filter; $g(\theta_{r,t}) = \frac{n^2}{\sin^2 \Phi}$ is the gain of the optical lens, with n and Φ being the refractive index and the half-angle field-of-view (FOV) of the optical lens, respectively; $\text{rect}(\varphi_{r,t}, \theta_{r,t}, \Psi, \Phi)$ is the rectangular function, which is defined by

$$\text{rect}\left(\varphi_{r,t}, \theta_{r,t}, \Psi, \Phi\right) = \begin{cases} 1, & 0 \le \varphi_{r,t} \le \Psi \text{ and } 0 \le \theta_{r,t} \le \Phi \\ 0, & \varphi_{r,t} > \Psi \text{ or } \theta_{r,t} > \Phi \end{cases}. \tag{5}$$

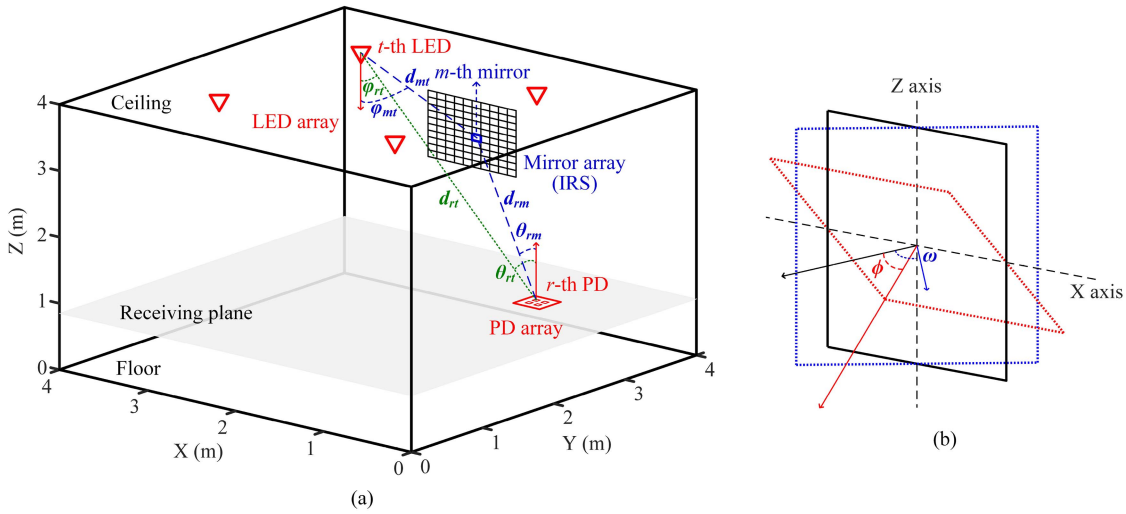

Fig. 1. Illustration of IRS-aided MIMO-VLC: (a) system model and (b) operation principle of the mirror unit in the IRS.

2) NLOS Channel Gain: The NLOS channel gain is mainly caused by the diffuse reflection of the walls, and the NLOS channel gain between the r-th PD and the t-th LED due to the diffuse reflection of the i-th reflective point can be obtained by [12], [36]

$$h_{r,t}^{\mathrm{NLOS}} = \int \frac{(l+1)\rho A\varepsilon}{2(\pi d_{i,t} d_{r,i})^2} \cos^l(\varphi_{i,t}) \cos(\alpha_{i,t}) \cos(\beta_{r,i}) T_s \times g(\theta_{r,i}) \cos(\theta_{r,i}) \mathrm{rect}(\varphi_{i,t}, \theta_{r,i}, \Psi, \Phi) dA_{\mathrm{wall}}, \quad (6)$$

where ε is the reflectance coefficient of the wall; $d_{i,t}$ is the distance between the i-th reflective point and the t-th LED; $d_{r,i}$ is the distance between the r-th PD and the i-th reflective point; $\varphi_{i,t}$ and $\alpha_{i,t}$ are the emission angle and the incident angle from the t-th LED to the i-th reflective point, respectively; $\beta_{r,i}$ and $\theta_{r,i}$ are the emission angle and the incident angle from the i-th reflective point to the r-th PD, respectively; $\mathrm{rect}(\varphi_{i,t}, \theta_{r,i}, \Psi, \Phi)$ is the corresponding rectangular function; dA_{wall} is a small reflective area on the wall.

3) IRS Channel Gain: As shown in Fig. 1(a), a mirror array-based IRS is placed on the wall to modify the MIMO channel. In the IRS equipped with multiple rotatable mirror units, each mirror unit can be rotated to a pre-defined orientation and hence can serve as a specular reflector to reflect the light emitted from a specific LED to a target PD [24]. More specifically, as shown in Fig. 1(b), the orientation of the rotatable mirror unit can be efficiently controlled by the azimuth angle ω and the polar angles ϕ through the micro-electro-mechanical systems (MEMS) technology in real-world scenarios [37]. Let $h_{r,m,t}^{\mathrm{IRS}}$ denote the IRS channel gain between the r-th PD and the t-th LED, which is reflected by the m-th ($m = 1, 2, \ldots, M$) mirror unit, in the MIMO-VLC system employing an IRS with totally M mirror units. Under the point source assumption, the IRS channel gain can be approximated by [25]

$$h_{r,m,t}^{\mathrm{IRS}}(\lambda_{r,m,t}) = \frac{(l+1)\rho A\delta\lambda_{r,m,t}}{2\pi(d_{m,t}+d_{r,m})^2} \cos^l(\varphi_{m,t}) T_s g(\theta_{r,m}) \times \cos(\theta_{r,m}) \mathrm{rect}(\varphi_{m,t}, \theta_{r,m}, \Psi, \Phi), \quad (7)$$

where δ is the reflectance coefficient of the IRS mirror unit; $d_{m,t}$ is the distance between the m-th IRS mirror unit and the t-th LED; $d_{r,m}$ is the distance between the r-th PD and the m-th IRS mirror unit; $\varphi_{m,t}$ is the emission angle from the t-th LED to the m-th IRS mirror unit; $\theta_{r,m}$ is the incident angle from the m-th IRS mirror unit to the r-th PD; $\mathrm{rect}(\varphi_{r,m,t}, \theta_{r,m,t}, \Psi, \Phi)$ is the corresponding rectangular function. Moreover, $\lambda_{r,m,t}$ denotes the mirror assignment coefficient of the m-th mirror to the sub-channel between the r-th PD and the t-th LED. It can be seen from (7) that the IRS channel gain is inversely proportional to the square of the sum of the distances, which indicates that the reflected light can be considered as that emitted from a corresponding imaging LED [25]:

B. Noise Model

The additive noise in the IRS-aided MIMO-VLC system usually consists of both shot and thermal noises, which can be reasonably modeled as a real-valued zero-mean additive white Gaussian noise (AWGN) with power $P_n = N_0 B$, where N_0 and B denote the noise power spectral density (PSD) and the modulation bandwidth, respectively [12].

C. MIMO Transmission Techniques

We consider three typical MIMO transmission techniques in the IRS-aided MIMO-VLC system, including RC, SM and SMP.

1) RC: As the simplest MIMO transmission technique, RC can achieve high diversity gain by using all the transmitters to transmit the same signal [6], [11]. Nevertheless, the spectral efficiency of RC-based MIMO-VLC systems is relatively low.

2) SM: SM is a digitized MIMO transmission scheme, which activates only one of the transmitters to transmit the conventional constellation symbol at each time slot and the selection of the activated transmitter can also encode additional bits [5]. Hence, SM can transmit not only conventional constellation symbols

but also additional spatial bits. Since only a single transmitter is activated for signal transmission at each time slot, SM enjoys the inherent advantages of negligible inter-channel interference (ICI), high power efficiency and low transceiver complexity [9]. However, it is very challenging for SM-based MIMO-VLC systems to achieve high spectral efficiency.

3) SMP: SMP is the most widely applied MIMO transmission technique in VLC systems, which activates all the transmitters to transmit different signals independently. As a result, SMP can harvest multiplexing gain under the condition of non-negligible ICI [8], [38]. Compared with RC and SM, SMP can achieve relatively high spectral efficiency.

III. Optimization of Surface Configuration in IRS-Aided MIMO-VLC

In an IRS-aided MIMO-VLC system, the IRS component of the channel matrix, i.e., $\mathbf{H}_{\text{IRS}}$, is determined by the configuration of all the mirror units in the mirror array-based IRS. More specifically, as given in (7), $\mathbf{H}_{\text{IRS}}$ can be characterized based on the alignment of each mirror unit in the IRS with a corresponding LED/PD pair [23]. In this section, we aim to minimize the BER of the IRS-aided MIMO-VLC system by optimizing the surface configuration of the IRS.

A. Problem Formulation

We employ the maximum-likelihood (ML) detection in the IRS-aided MIMO-VLC system to achieve optimal performance. Consequently, we derive an analytical error bound for ML detection, resulting in an explicit expression that can be represented as [6], [39], [40]

$$P_b \leq \frac{1}{2^{\eta}\eta} \sum_{\mathbf{x}} \sum_{\hat{\mathbf{x}}} d_{\text{H}}\left(\mathbf{x}, \hat{\mathbf{x}}\right) P_e\left(\mathbf{x} \to \hat{\mathbf{x}}, \gamma_{\text{tx}}\right), \tag{8}$$

where η denotes the spectral efficiency, $d_{\text{H}}(\mathbf{x}, \hat{\mathbf{x}})$ represents the Hamming distance between signal vectors $\mathbf{x}$ and $\hat{\mathbf{x}}$, and P_e is the pairwise error probability (PEP), denoting the likelihood of the receiver mistaking the transmitted signal vector $\mathbf{x}$ for $\hat{\mathbf{x}}$ given a specific transmitted signal-to-noise ratio (SNR) γ_{tx}. It is worth noticing that transmitted SNR is defined as the ratio of the transmitted electrical signal power to the additive noise power, which is generally adopted in MIMO-VLC systems for a fair BER performance evaluation [6], [11], [12]. Moreover, $P_e(\mathbf{x} \to \hat{\mathbf{x}})$ can be simplified as [41]

$$P_e\left(\mathbf{x} \to \hat{\mathbf{x}}, \gamma_{\text{tx}}\right) \leq \frac{1}{6} e^{-\frac{\|\mathbf{Hc}\|^2}{2}\gamma_{\text{tx}}} + \frac{1}{12} e^{-\frac{\|\mathbf{Hc}\|^2}{4}\gamma_{\text{tx}}} + \frac{1}{4} e^{-\frac{\|\mathbf{Hc}\|^2}{8}\gamma_{\text{tx}}}, \tag{9}$$

where $\mathbf{c} = \mathbf{x} - \hat{\mathbf{x}}$ represents the difference between $\mathbf{x}$ and $\hat{\mathbf{x}}$. It has been verified in [40] that this BER upper bound closely aligns with the simulation BER in the high-SNR regions.

In the IRS-aided MIMO-VLC system, the channel matrix $\mathbf{H}$ can be efficiently modified by the adopted IRS. Let $\boldsymbol{\lambda} \triangleq (\lambda_{r,m,t})_{r\in\mathcal{R},m\in\mathcal{M},t\in\mathcal{T}}$ denote the mirror assignment strategy with $\lambda_{r,m,t}$ being the mirror assignment coefficient of the m-th mirror to the sub-channel between the r-th PD and the t-th LED. Referring to (8) and (9), the BER upper bound can be expressed by (10) shown at the bottom of this next page, which is a function of $\boldsymbol{\lambda}$ as shown at the top of the next page. Note that the majority of parameters in (10) are fixed, except for the channel matrix $\mathbf{H}$, which solely depends on the mirror assignment strategy $\boldsymbol{\lambda}$. Therefore, we can formulate the optimization problem as follows.

Problem 1 (BER Minimization Problem):

$$\min_{\boldsymbol{\lambda}} f(\boldsymbol{\lambda}),$$

s.t.

$$\sum_{r\in\mathcal{R},t\in\mathcal{T}} \lambda_{r,m,t} = 1, \quad m \in \mathcal{M}, \tag{11}$$

$$\lambda_{r,m,t} \in \{0,1\}, \quad r \in \mathcal{R}, t \in \mathcal{T}, m \in \mathcal{M}. \tag{12}$$

The constraint in (11) guarantees that each mirror is assigned to only one sub-channel, while (12) signifies whether a mirror has been assigned or not. However, Problem 1 is an integer nonlinear programming problem and is non-deterministic polynomial-time hard (NP-hard) in general. This makes it difficult to find an optimal solution. Hence, in the following, we would like to propose a low-complexity algorithm to solve Problem 1.

B. Problem Solution

Our proposed algorithm to tackle Problem 1 is composed of three essential components: continuous relaxation and variable transformation, binary rounding, and feasible projection. We will provide a detailed explanation of these components in this subsection.

1) Continuous Relaxation and Variable Transformation: By relaxing the binary constraint in (12) to

$$\lambda_{r,m,t} \in [0,1], \tag{13}$$

we can obtain a continuous relaxation problem of Problem 1, as follows.

Problem 2 (Continuous Relaxation of Problem 1):

$$\boldsymbol{\lambda}^* \triangleq \arg\min_{\boldsymbol{\lambda}} f(\boldsymbol{\lambda}),$$

s.t. (11), (13).

Problem 2 is a continuous optimization problem with linear constraints and as such, can be solved using an interior point method. However, the computational complexity is high due to the considerable number of polynomials in (10), with each polynomial containing $N_t N_r M$ variables. To address this challenge, we replace the variable $\boldsymbol{\lambda}$ of Problem 2 to the channel gain $\tilde{\mathbf{H}}$, given by

$$\tilde{\mathbf{H}} = \begin{pmatrix} \tilde{h}_{1,1} & \cdots & \tilde{h}_{1,N_t} \\ \vdots & \ddots & \vdots \\ \tilde{h}_{N_r,1} & \cdots & \tilde{h}_{N_r,N_t} \end{pmatrix}, \tag{14}$$

where $\tilde{h}_{i,j}$ indicates the channel gain between the i-th PD and the j-th LED. As a result, we obtain a low-complexity solution of Problem 2, i.e.,

Algorithm 1: Binary Rounding.

Input: M, $\hat{\boldsymbol{\lambda}}^*$, Δ_P, ζ, α_p, $\alpha_{\max}$, ϵ.
Output: $\boldsymbol{\rho}_1, \boldsymbol{\rho}_2, \cdots, \boldsymbol{\rho}_Q$
Set $\alpha_p := 0$, $\epsilon := 0$
while $\alpha_p \leq \alpha_{\max}$ **do**
  Generate $\hat{\mathbf{x}}_{\mathbf{e}}^* \triangleq (x_j)_{j=1,2,\ldots,N_t N_r M}$ according to

$$x_j = \begin{cases} \lambda_j^*, & \text{if } \lambda_j^* > \alpha_p, \\ 0, & \text{if } \lambda_j^* \leq \alpha_p, \end{cases} \quad j = 1, 2, \ldots, N_t N_r M.$$

  Set $M_{\mathrm{n}}^{\epsilon}$ to the number of non-zero variables in $\hat{\mathbf{x}}_{\mathbf{e}}^*$.
  if $M_{\mathrm{n}}^{\epsilon} < M$ **then**
    Go to Step 16.
  else if $M_{\mathrm{n}}^{\epsilon} = M_{\mathrm{n}}^{\epsilon-1}$ **then**
    Set $\alpha_p := \alpha_p + \Delta_p$, $\epsilon := \epsilon + 1$. And go to Step 4
  else
    Generate solution $\boldsymbol{\rho}_q$ from $\hat{\mathbf{x}}_{\mathbf{e}}^*$ for all $q = 1, 2, \ldots, \zeta$ according to the following rule: Randomly select M numbers from the set of non-zero values of $\hat{\mathbf{x}}_{\mathbf{e}}^*$ with equal probability $\frac{1}{M_{\mathrm{n}}^{\epsilon}}$ and set them the value of 1, while setting the remaining values to 0
    Set $\alpha_p := \alpha_p + \Delta_p$, $\epsilon := \epsilon + 1$.
  end if
end while
Obtain the all assignment strategy vectors $\boldsymbol{\rho}_1, \boldsymbol{\rho}_2, \cdots, \boldsymbol{\rho}_Q$.

Problem 3 (Low-complexity Solution of Problem 2):

$$\tilde{\mathbf{H}}^* \triangleq \arg\min_{\tilde{\mathbf{H}}} f\left(\tilde{\mathbf{H}}\right),$$

$$\text{s.t.} \sum_{i\in\mathcal{R}, j\in\mathcal{T}} \tilde{h}_{i,j} \leq h_{\max}^{\mathrm{IRS}} + h_{\mathrm{P}}^{\mathrm{LOS}} + h_{\mathrm{P}}^{\mathrm{NLOS}}, \tag{15}$$

$$\tilde{h}_{i,j}^{\mathrm{LOS}} + \tilde{h}_{i,j}^{\mathrm{NLOS}} \leq h_{i,j} \leq \tilde{h}_{i,j}^{\mathrm{LOS}} + \tilde{h}_{i,j}^{\mathrm{NLOS}} + \tilde{h}_{i,j}^{\mathrm{IRS}}, \quad i \in \mathcal{R}, j \in \mathcal{T}. \tag{16}$$

Here, $\tilde{\mathbf{H}}^*$ represents an optimal solution. The equation $f(\mathbf{h})$ corresponds to the equation $f(\boldsymbol{\lambda})$, which transforms the variable $\boldsymbol{\lambda}$ to $\mathbf{h}$. Constraint (15) represents a restriction on the total channel gain, where $h_{\max}^{\mathrm{IRS}}$ denotes the maximum IRS gain that the system can obtain using all mirrors. Additionally, $h_{\mathrm{P}}^{\mathrm{LOS}}$ and $h_{\mathrm{P}}^{\mathrm{NLOS}}$ signify the sum of channel gains for the LOS and NLOS channels, respectively. For a specific position, both $h_{\mathrm{P}}^{\mathrm{LOS}}$ and $h_{\mathrm{P}}^{\mathrm{NLOS}}$ are constants. The constraint in (16) gives the upper and lower bounds on $\tilde{h}_{i,j}$, where $\tilde{h}_{i,j}^{\mathrm{LOS}}$ and $\tilde{h}_{i,j}^{\mathrm{NLOS}}$ are the LOS and NLOS channel gains of sub-channel between the i-th PD and the j-th LED. $\tilde{h}_{i,j}^{\mathrm{IRS}}$ is the channel gain when all mirrors are assigned to the sub-channel between the i-th PD and the r-th LED, which can be calculated using (7) for a given receiver position. However, Problem 3 is also difficult to solve directly, as calculating $h_{\max}^{\mathrm{IRS}}$ is considered NP-hard. Because solving $h_{\max}^{\mathrm{IRS}}$ is also an optimization problem similar to Problem 1. To tackle this challenge, we use the largest value of $\tilde{h}_{i,j}^{\mathrm{IRS}}$ as an approximation for $h_{\max}^{\mathrm{IRS}}$ and then solve Problem 3 approximately by using the sequential quadratic programming (SQP) method.

2) Binary Rounding: As suggested by (3), the IRS channel gain can be determined by subtracting the LOS and NLOS channels. Thus, we have

$$\mathbf{H}_0 = \tilde{\mathbf{H}}^* - (\mathbf{H}_{\mathrm{LOS}} + \mathbf{H}_{\mathrm{NLOS}}). \tag{17}$$

According to Section III-A, $\mathbf{H}_0$ can also be defined as

$$\mathbf{H}_0(\boldsymbol{\lambda}) = \begin{pmatrix} h_{1,1}^{\mathrm{IRS}}(\boldsymbol{\lambda}_{1,1}) & \cdots & h_{1,N_t}^{\mathrm{IRS}}(\boldsymbol{\lambda}_{1,N_t}) \\ \vdots & \ddots & \vdots \\ h_{N_r,1}^{\mathrm{IRS}}(\boldsymbol{\lambda}_{N_r,1}) & \cdots & h_{N_r,N_t}^{\mathrm{IRS}}(\boldsymbol{\lambda}_{N_r,N_t}) \end{pmatrix}, \tag{18}$$

where $h_{r,t}^{\mathrm{IRS}} = \boldsymbol{\lambda}_{r,t}^T \hat{\boldsymbol{h}}_{r,t}$ $(r \in \mathcal{R}, t \in \mathcal{T})$, and $\hat{\boldsymbol{h}}_{r,t} = (h_{r,1,t}^{\mathrm{IRS}}, h_{r,2,t}^{\mathrm{IRS}}, \ldots, h_{r,m,t}^{\mathrm{IRS}})^T$ is the channel gain vector of the sub-channel. Hence, we can get the assignment strategy by solving the following problem:

Problem 4:

$$\hat{\boldsymbol{\lambda}}^* \triangleq \arg\min_{\boldsymbol{\lambda}} \left\| \hat{\mathbf{H}}_0(\boldsymbol{\lambda}) - \mathbf{H}_0 \right\|_{\mathrm{F}}^2,$$

$$\text{s.t. (11), (13).}$$

The estimate $\hat{\boldsymbol{\lambda}}^*$ of $\hat{\boldsymbol{\lambda}}$ can be obtained by solving Problem 3, which uses the Frobenius norm to generate a matrix most similar to $\mathbf{H}_0$, subject to certain constraints. In general, Problem 3 can be viewed as a norm approximation problem with constraints, and it is solvable with at least one optimal solution [42]. Problem 4 is still a nonlinear problem, we also use the SQP method to solve it.

The optimal solution, $\hat{\boldsymbol{\lambda}}^* \triangleq (\lambda_{r,m,t}^*)_{r\in\mathcal{R}, t\in\mathcal{T}, m\in\mathcal{M}}$ of Problem 4 is generally non-binary and does not satisfy the constraint in (12). Nevertheless, it is also valuable as a reference. Each $\lambda_{r,m,t}^*$ represents the probability of assigning the m-th mirror to the sub-channel between the r-th PD and the t-th LED. By proposing a novel binary rounding method, we aim to generate multiple valid samples from $\hat{\boldsymbol{\lambda}}^*$ for the subsequent optimization step.

The details of the binary rounding process are presented in Algorithm 1. Several new parameters are introduced: $\alpha_{\max}$ is the largest value in $\hat{\boldsymbol{\lambda}}^*$; α_p represents the probability threshold; Δ_P is an increment; ζ denotes the number of solutions $\boldsymbol{\rho}_q$ generated per loop; M is number of mirrors; and $M_{\mathrm{n}}^{\epsilon}$ is the number of non-zero variables of $\hat{\mathbf{x}}_{\mathrm{e}}^*$ in the ϵ-th loops. In addition, we have redefined $\hat{\boldsymbol{\lambda}}^* \triangleq (\lambda_j^*)_{j=1,2,\ldots,N_t N_r M}$, only by modifying the corner markers to better represent it in the algorithm. The essence of Algorithm 1 is to execute a loop that ensures the generation of a sufficient number of valuable solutions. Specifically, Step 5 is to elect values in x that are greater than α_p, which refines the feasible set of solutions for $\hat{\boldsymbol{\lambda}}^*$ and enables the assignment strategy to concentrate on high-probability sets. Step 12 is the process of

$$f(\boldsymbol{\lambda}) = \frac{1}{2\eta\eta} \sum_{\mathbf{x}} \sum_{\hat{\mathbf{x}}} d_{\mathrm{H}}(\mathbf{x} \to \hat{\mathbf{x}}) \left(\frac{1}{6} e^{-\frac{\|\mathbf{H}(\boldsymbol{\lambda})\mathbf{c}\|^2}{2}\gamma_{\mathrm{tx}}} + \frac{1}{12} e^{-\frac{\|\mathbf{H}(\boldsymbol{\lambda})\mathbf{c}\|^2}{4}\gamma_{\mathrm{tx}}} + \frac{1}{4} e^{-\frac{\|\mathbf{H}(\boldsymbol{\lambda})\mathbf{c}\|^2}{8}\gamma_{\mathrm{tx}}} \right). \tag{10}$$

Algorithm 2: The Overall Algorithm for Solving Problem 1.

1: **Input:** $h_{\max}^{\mathrm{IRS}}$, $h_{\mathrm{P}}^{\mathrm{LOS}}$, $h_{\mathrm{P}}^{\mathrm{NLOS}}$, $\tilde{h}_{i,j}^{\mathrm{LOS}}$, $\tilde{h}_{i,j}^{\mathrm{NLOS}}$, $\tilde{h}_{i,j}^{\mathrm{IRS}}$
2: **Output:** $\boldsymbol{\lambda}^*$
3: Determine $\mathbf{H}^*$ of Problem 3 via the SQP method using input parameters.
4: Determine $\hat{\boldsymbol{\lambda}}^*$ of Problem 4 via the SQP method.
5: Obtain $\boldsymbol{\rho}_s$ for all $s \in \mathcal{Q}$ using Algorithm 1.
6: Obtain $\hat{\boldsymbol{\rho}}_s^{\S}$ for all $s \in \mathcal{Q}$ using an interior-point method.
7: Calculate $\boldsymbol{\lambda}^*$ via (27).

generating solutions, generating ζ solutions per loop. And Steps 6 to 11 are the early exit conditions, which prevent unnecessary loops and repeated searches. Finally, we obtained all the solutions $(\boldsymbol{\rho}_s \triangleq (p_{s,n})_{n\in\mathcal{N}}, s = 1, 2, \ldots, \zeta, \zeta+1, \ldots, Q)$, which are composed of the solution $\boldsymbol{\rho}_q$ in each loop.

We now discuss the complexity of the proposed algorithm. For Algorithm 1, its computational complexity depends on how many loops it has executed. Specifically, in the worst case, we need to execute $\lfloor \frac{\alpha_{\max}}{\Delta_p} \rfloor + 1$ loops, and every loop has $N_r N_t M + \delta M$ assignment operations. Hence, it performs at most $(\lfloor \frac{\alpha_{\max}}{\Delta_p} \rfloor + 1)(N_r N_t M + \zeta M)$ times assignment operations when every loop can generate an effective solution. Note that the algorithm's actual complexity is significantly lower, and we will demonstrate this in the subsequent section.

3) Feasible Projection: The solutions $\boldsymbol{\rho}_s$ generated from Algorithm 1 satisfy the constraint in (12), but they may not satisfy the constraint in (11). Therefore, to construct a solution that satisfies both the constraints, we employ a feasible projection method [43], [44], with its problem formulated as:

Problem 5 (Feasible Projection):

$$\hat{\boldsymbol{\rho}}_s^* \triangleq \arg\min_{\hat{\boldsymbol{\rho}}_s} \|\hat{\boldsymbol{\rho}}_s - \boldsymbol{\rho}_s\|_2^2,$$
$$\text{s.t. (11), (12),} \tag{19}$$

where $\hat{\boldsymbol{\rho}}_s^* \triangleq (\hat{\rho}_{s,n}^*)_{n\in\mathcal{N}}$ denotes an optimal solution. Problem 5 is an integer nonlinear programming problem, generally considered NP-hard. However, since $\|\hat{\boldsymbol{\rho}}_s - \boldsymbol{\rho}_s\|_2^2$ can be rewritten as the sum of $N_t N_r M$ single-variable integer convex functions, i.e., $\|\hat{\boldsymbol{\rho}}_s - \boldsymbol{\rho}_s\|_2^2 = \sum_{n\in\mathcal{N}} (\hat{\rho}_{s,n} - \rho_{s,n})^2$, and each single-variable integer convex function $\hat{\rho}_{s,n} - \rho_{s,n}$ can be replaced by an equivalent linear problem:

$$\hat{\rho}_{s,n} - \rho_{s,n} = \min_{a_{s,n}, b_{s,n}} \rho_{s,n}^2 a_{s,n} + (1-\rho_{s,n})^2 b_{s,n},$$
$$\text{s.t. (11), (12),}$$
$$b_{s,n} = \hat{\rho}_{s,n} \quad s \in \mathcal{Q}, n \in \mathcal{N}, \tag{20}$$
$$a_{s,n} + b_{s,n} = 1, \quad s \in \mathcal{Q}, n \in \mathcal{N}, \tag{21}$$
$$a_{s,n} > 0, a_{s,n} > 0, \quad s \in \mathcal{Q}, n \in \mathcal{N}. \tag{22}$$

Hence, we can equivalently rewrite Problem 5 as [43], [44]:

$$(\hat{\boldsymbol{\rho}}_s^{\S}, \boldsymbol{a}_s^{\S}, \boldsymbol{b}_s^{\S}) \triangleq \arg\min_{a_{s,n}, b_{s,n}} \sum_{n\in\mathcal{N}} \rho_{s,n}^2 a_{s,n} + (1-\rho_{s,n})^2 b_{s,n}, \tag{23}$$
$$\text{s.t. (11), (12),}$$
$$b_{s,n} = \rho_{s,n}^{\S} \quad s \in \mathcal{Q}, n \in \mathcal{N}, \tag{24}$$
$$a_{s,n} + b_{s,n} = 1, \quad s \in \mathcal{Q}, n \in \mathcal{N}, \tag{25}$$
$$a_{s,n} > 0, a_{s,n} > 0, \quad s \in \mathcal{Q}, n \in \mathcal{N}. \tag{26}$$

Here, $\boldsymbol{a}_s^{\S} \triangleq (a_{s,n})_{n\in\mathcal{N}}$, $\boldsymbol{b}_s^{\S} \triangleq (b_{s,n})_{n\in\mathcal{N}}$, and $(\hat{\boldsymbol{\rho}}_s^{\S}, \boldsymbol{a}_s^{\S}, \boldsymbol{b}_s^{\S})$ denotes an optimal solution. We input all solutions $\hat{\boldsymbol{\rho}}_s^{\S}$ into (10) to calculate Q BERs:

$$\boldsymbol{\lambda}^* \triangleq \arg\min_{\hat{\boldsymbol{\rho}}_s^{\S}} f\left(\hat{\boldsymbol{\rho}}_s^{\S}\right), \tag{27}$$

and the solution corresponding to the smallest BER of $\hat{\boldsymbol{\rho}}_s^{\S}$ is considered a good feasible solution $\boldsymbol{\lambda}^*$.

4) Algorithm Summary: As mentioned above, we are now ready to present the overall algorithm for solving Problem 1, as summarized in Algorithm 2. The total computational complexity of Algorithm 2 is determined by the cumulative computational complexities of the four aforementioned phases: Problems 3, 4, 5, and Algorithm 1. Of these phases, the computational complexity of the SQP algorithm primarily lies in solving the quadratic programming (QP) subproblem, typically operating at an order of $\mathcal{O}(V^3)$, where V represents the number of variables. Consequently, the computation complexity of Problems 3 and 4 can be expressed as $\mathcal{O}(M^3)$ and $\mathcal{O}((N_r N_t M)^3)$, respectively. In addition, the SQP method, as a classic algorithm, has been extensively studied and is widely recognized for its ability to handle nonlinear problems. As depicted in Fig. 2, the SQP method exhibits favorable convergence properties, typically achieving convergence within 10 iterations for Problems 3 and 4. Notably, the utility of the method demonstrates a significant improvement during the initial 3 iterations, followed by a stable performance sustained over 10 iterations.

Lastly, it is also worth noticing that Problem 5 in (23) is a linear programming problem, and therefore its optimal solution can be efficiently attained by using the interior-point method, which has the computation complexity of $\mathcal{O}((3N_r N_t M)^{3.5} \log(1/\varepsilon))$, where $3N_r N_t M$ is the total number of variables, $(3N_r N_t M)^{3.5}$ is the complexity order of dominant Hessian matrix calculation, and ε is the solution accuracy [45]. Additionally, the complexity of Algorithm 1 has been previously discussed. To sum up, the total computational complexity of Algorithm 2 is the sum of the computational complexity of the aforementioned four phases, which is given by $\mathcal{O}(M^3 + (N_r N_t M)^3 + (3N_r N_t M)^{3.5} \log(1/\varepsilon) + (\lfloor \frac{\alpha_{\max}}{\Delta_p} \rfloor + 1)(N_r N_t M + \zeta M)))$. It is crucial to highlight that Algorithm 1 yielded a significantly lower complexity due to Steps 6 to 11. As depicted in Fig. 3, the actual complexity amounts to a mere 14.8% of the maximum complexity.

IV. Results and Discussions

In this section, we evaluate and compare the BER performance of the IRS-aided MIMO-VLC system applying three MIMO techniques (i.e., RC, SM, and SMP) under different IRS configurations.

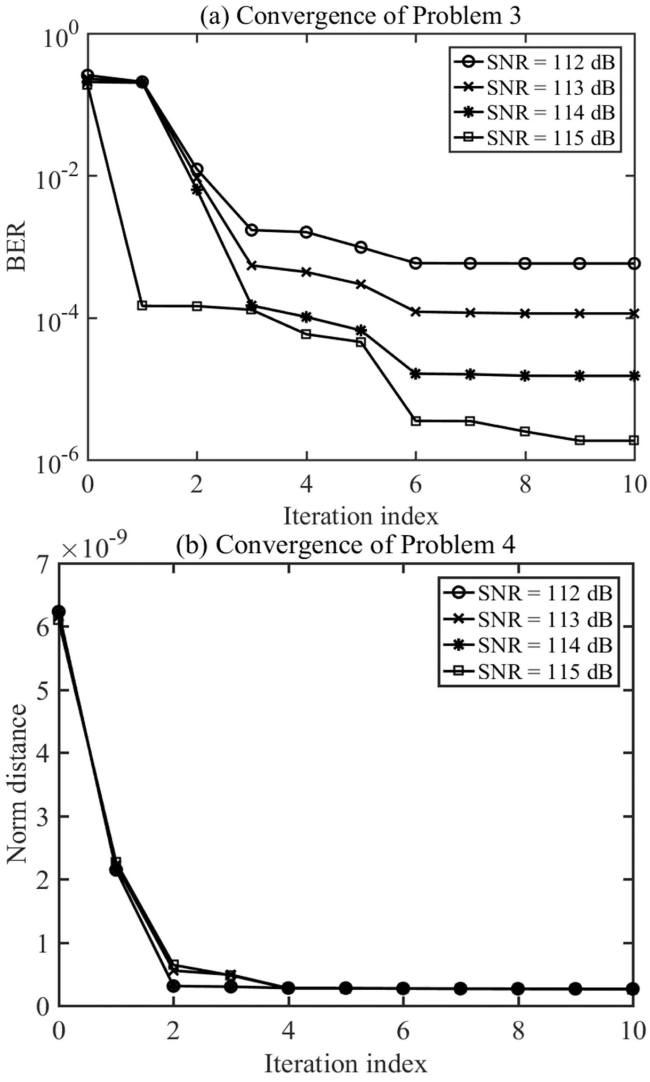

Fig. 2. Convergence using the SQP method for SMP with $M = 16$ at PD position 1: (a) Problem 3 and (b) Problem 4.

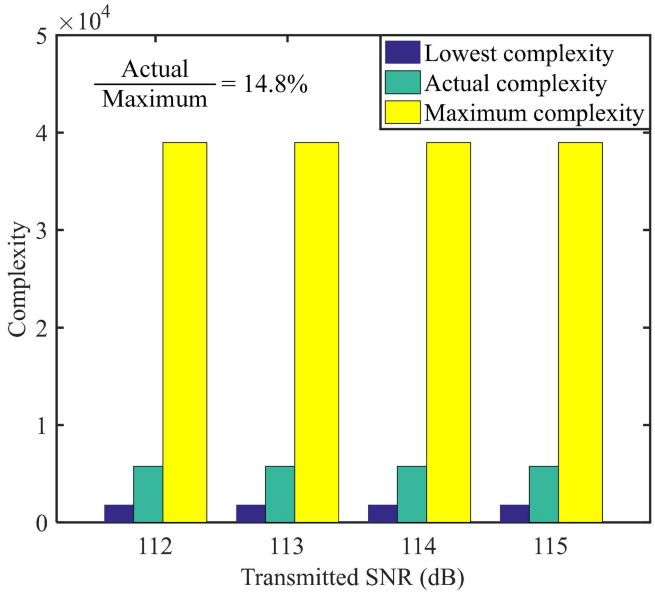

Fig. 3. Actual complexity of Algorithm 1. The simulation parameters are set as $\Delta_p = 0.05$ and $\delta = 100$.

TABLE I
FIX PARAMETERS OF IRS ADDING VLC SYSTEM

Parameter	Value
Room dimension	4 m × 4 m × 4 m
Height of receiving plane	0.85 m
LED positions	(1 m, 1 m, 4 m), (1 m, 3 m, 4 m), (3 m, 1 m, 4 m), (3 m, 3 m, 4 m)
PD array position 1	(1.5 m, 2 m, 0.85 m)
PD array position 2	(2 m, 2 m, 0.85 m)
PD array position 3	(2.5 m, 2 m, 0.85 m)
Semi-angle at half power of LED, Ψ	90°
Half-angle FOV of optical lens, Φ	90°
LED spacing	2 m
Gain of optical filter, T_s	0.9
Responsivity of APD, ρ	15 A/W
Active area of APD, A	1 cm^2
APD spacing	10 cm
Reflectance coefficient of wall, ε	0.8
Reflectance coefficient of mirror, δ	0.9
Noise power spectral density, N_0	10^{-22} A^2/Hz
LED modulation bandwidth, B	20 MHz

A. Simulation Setup

In our simulations, we set up a 4×4 MIMO-VLC system in a typical indoor room, where the room has a dimension of 4 m × 4 m × 4 m and the receiving plane is 0.85 m above the floor. The LED array is mounted at the ceiling and the user equipped with a PD array is located over the receiving plane. Moreover, the mirror array-based IRS is located on the side wall consisting of multiple square-shaped mirror units, with the IRS center position being (4 m, 2 m, 2 m). Each square-shaped mirror unit has a side length of 1 cm and the spacing between two adjacent mirro units is 10 cm. Without loss of generality, we assume 4-ary pulse amplitude modulation (4-PAM) is used for all three MIMO techniques, and hence the spectral efficiencies achieved by RC, SM, and SMP are 2, 4, and 8 bits/s/Hz, respectively. Moreover, the IRS is assumed to be a square-shaped mirror array with total M mirror units, where two M values, i.e., $M =$ 16 and 36, are considered in the following evaluations. The key parameters of the 4×4 MIMO-VLC system are listed in Table I. In addition, perfect channel state information (CSI) is assumed to be known at the transmitter side to execute the optimization of the IRS configuration. Since the received SNRs corresponding to different LED/PD pairs might be different in the MIMO-VLC system, the transmitted SNR is adopted as the figure of merit to evaluate the BER performance of MIMO-VLC systems, which is defined in decibel (dB) as $\text{SNR}_{\text{Tx}} = 10\log_{10}(\frac{P_s}{P_n})$ [12]. Hence, the transmitted optical power P_s of each LED is calculated according to the noise power P_n and the transmitted SNR SNR_{Tx} as follows:

$$P_s = 10^{\frac{\text{SNR}_{\text{Tx}}}{10}} P_n. \tag{28}$$

1) Optimization Tools: The optimization is performed by using the MATLAB software. In particular, our algorithm mainly solves Problems 3, 4, and 5. For Problems 3 and 4, we employ

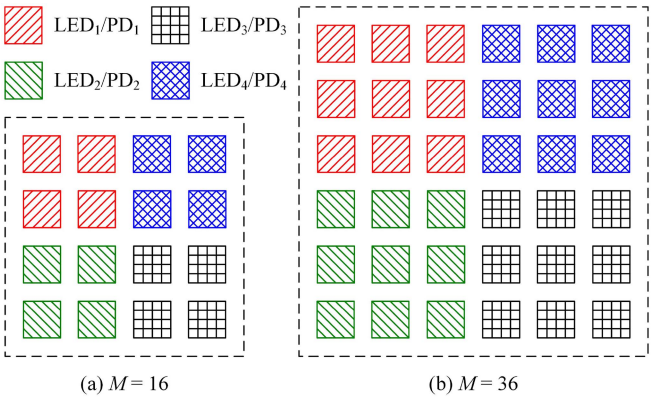

Fig. 4. The baseline IRS configuration: (a) $M = 16$ and (b) $M = 36$.

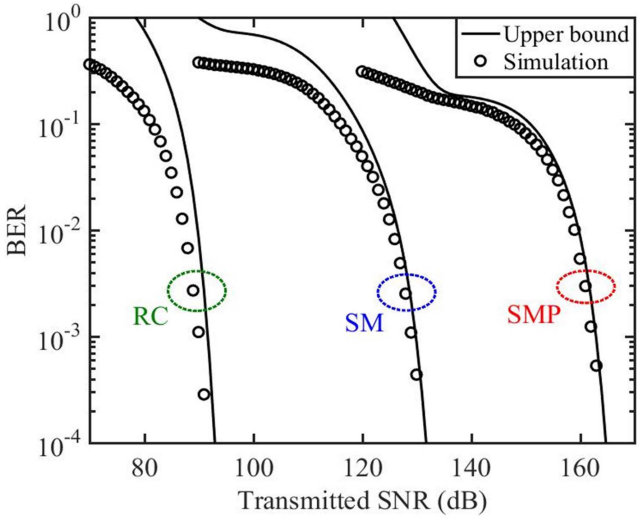

Fig. 5. BER performance of the 4×4 MIMO-VLC system applying different MIMO techniques without utilizing IRS at PD array position 2.

the interior point method to solve them. For Problem 5, we utilize the CVX toolbox with the MOSEK solver to address it. The optimization is individually performed for each given transmitted SNR.

2) Baseline Settings: To demonstrate the superiority of our proposed optimization algorithm, we compare it to a representative baseline scheme that assigns the mirror units equally to the LED/PD channels. Fig. 4(a) and (b) depict the IRS configurations for the baseline scheme with $M = 16$ and 36, respectively. As we can see, when applying the baseline scheme, all the mirror units are equally divided into four regions and each region is allocated to a corresponding LED/PD channel. As a result, the obtained IRS component of the channel matrix becomes a diagonal channel matrix which can be expressed as follows:

$$\mathbf{H}_{\mathrm{IRS}}^{\mathrm{Baseline}} = \begin{bmatrix} h_{11,\mathrm{IRS}}^{\mathrm{Baseline}} & & \\ & \ddots & \\ & & h_{44,\mathrm{IRS}}^{\mathrm{Baseline}} \end{bmatrix}. \tag{29}$$

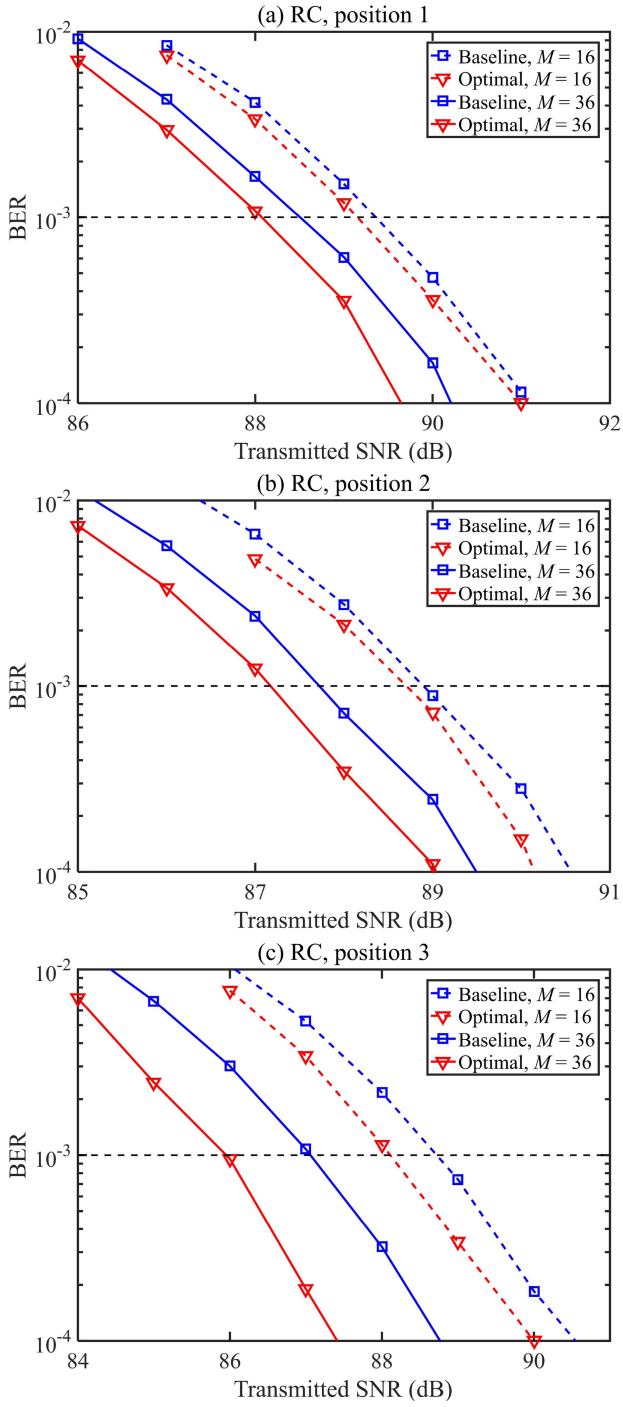

Fig. 6. BER vs. transmitted SNR for the IRS-aided 4×4 MIMO-VLC system applying RC at different PD array positions: (a) position 1, (b) position 2, and (c) position 3.

B. BER Performance

We first evaluate the BER performance of the 4×4 MIMO-VLC system applying different MIMO techniques without utilizing IRS. Fig. 5 shows the analytical BER upper bounds and the simulated BERs versus transmitted SNR at PD position 2. It can be observed that, for all three MIMO techniques including RC, SM and SMP, the analytical BER upper bounds closely match the

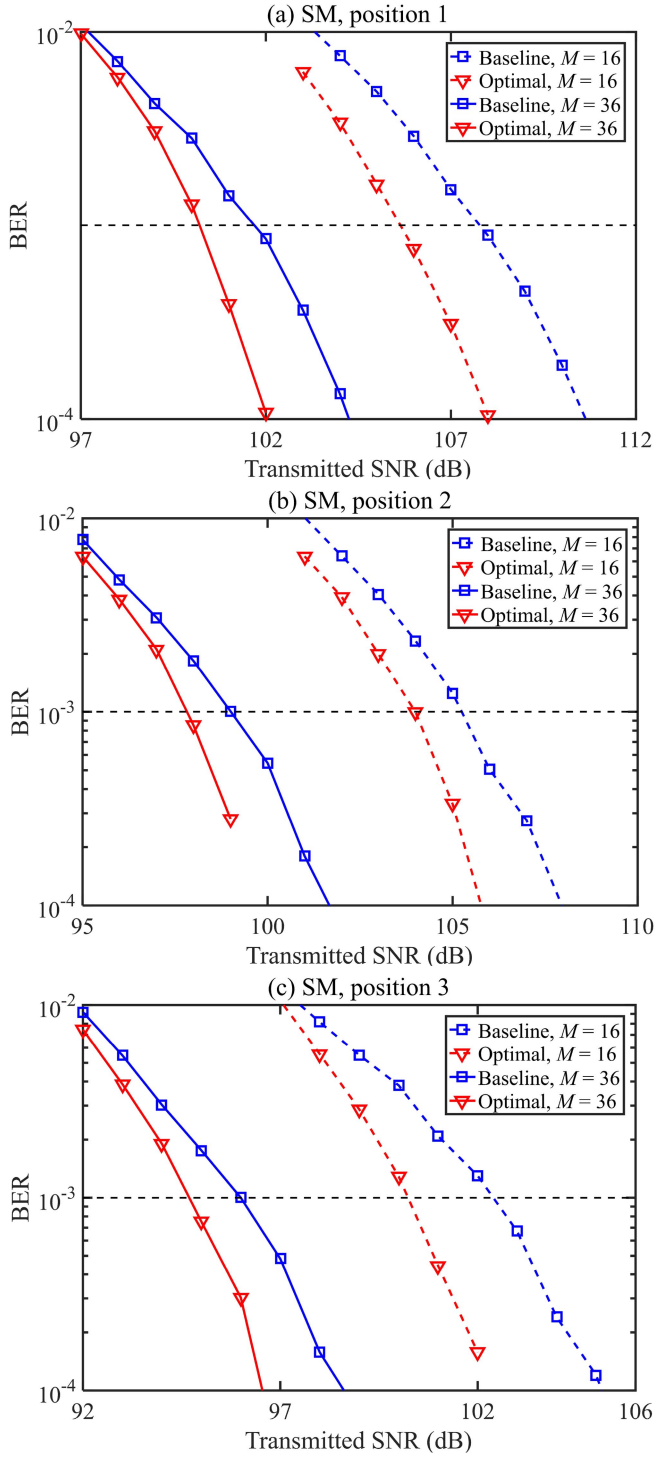

Fig. 7. BER vs. transmitted SNR for the IRS-aided 4×4 MIMO-VLC system applying SM at different PD array positions: (a) position 1, (b) position 2, and (c) position 3.

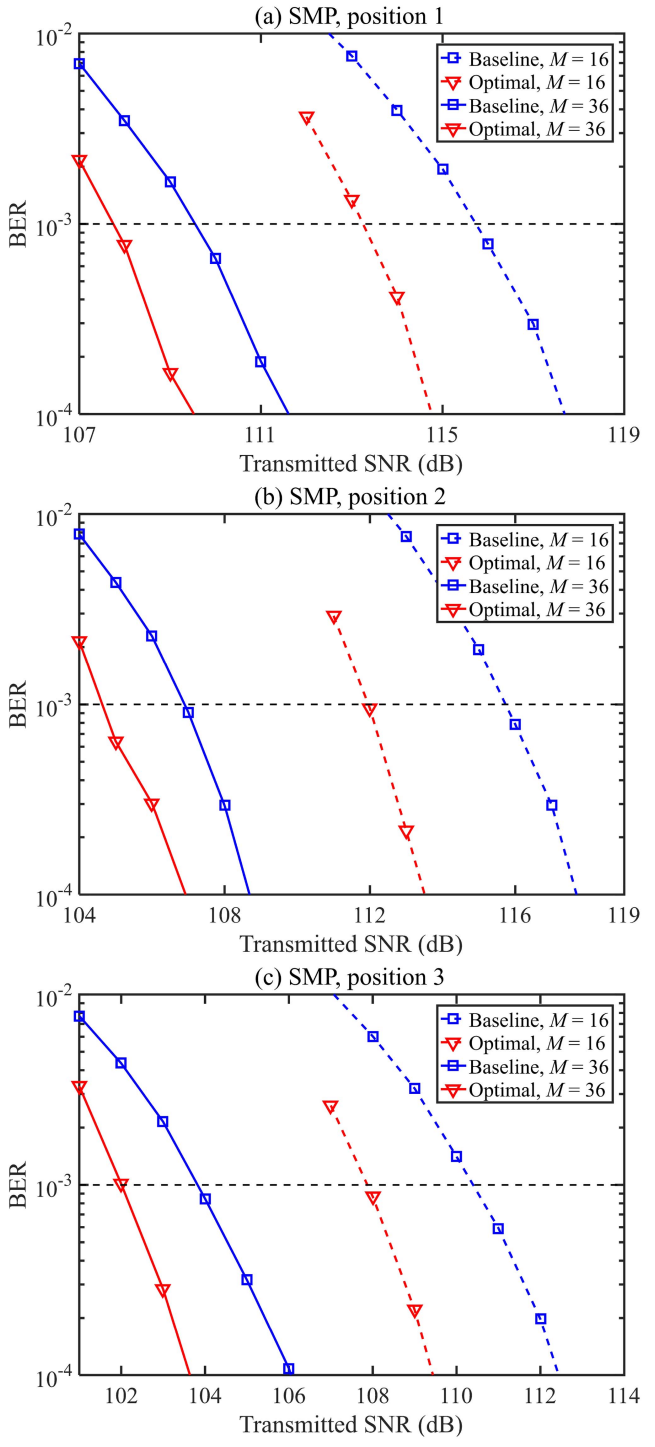

Fig. 8. BER vs. transmitted SNR for the IRS-aided 4×4 MIMO-VLC system applying SMP at different PD array positions: (a) position 1, (b) position 2, and (c) position 3.

simulated BER when the SNRs are relatively large. Therefore, the analytical BER upper bounds are verified to be very tight at the high SNR regions, which can be efficiently used to perform IRS configuration optimization in the IRS-aided MIMO-VLC systems applying different MIMO techniques. Moreover, the required transmitted SNRs for RC, SM and SMP to reach BER $= 10^{-3}$ are about 90, 130 and 160 dB, respectively. And as a reference, in our simulation setup, the channel coefficients are in the region of 10^{-4}, the path loss at the receiver side is about -80 dB. Hence, relatively large SNRs are required to achieve satisfactory transmission performance when the IRS is not introduced in the 4×4 MIMO-VLC system, especially for the SMP scheme, due to the adverse effect of channel correlation [11].

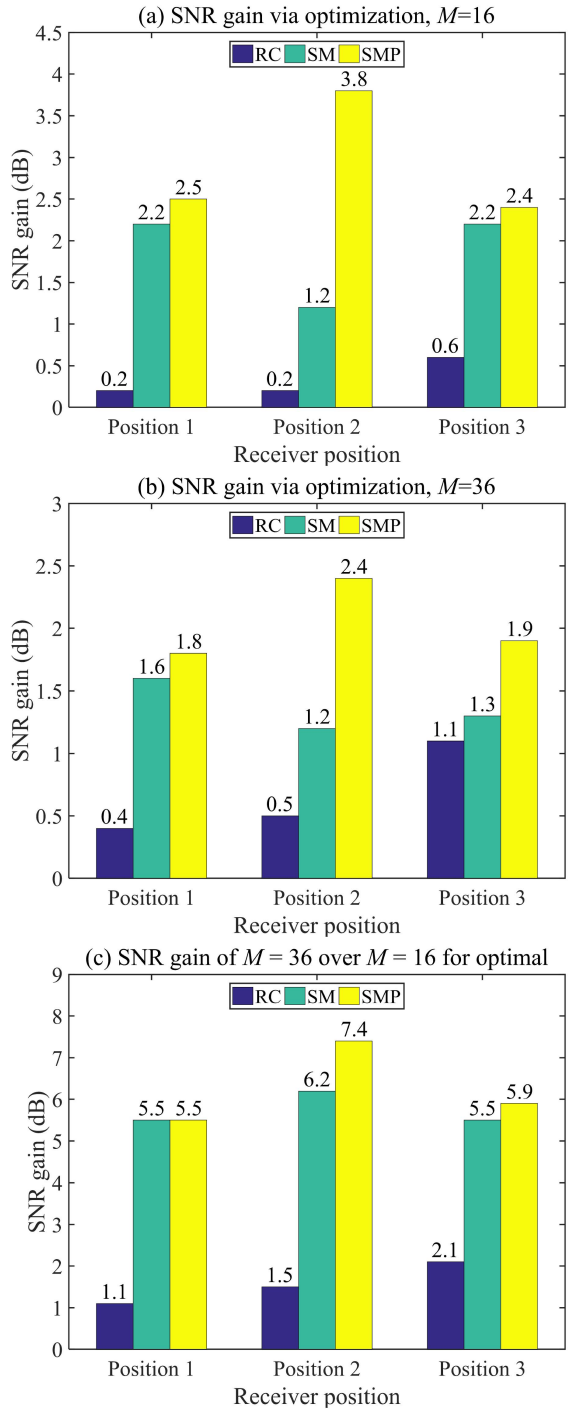

Fig. 9. SNR gain at different PD array positions: (a) the optimal scheme over the baseline scheme for $M = 16$, (b) the optimal scheme over the baseline scheme for $M = 36$, and (c) $M = 36$ over $M = 16$ for the optimal scheme.

In the next, we investigate the BER performance of the IRS-aided 4×4 MIMO-VLC system applying different MIMO techniques. Fig. 6 shows the BER versus transmitted SNR for the IRS-aided 4×4 MIMO-VLC system applying RC at different PD positions. As we can see, at given PD array positions, the SNR gain obtained by the optimal scheme in comparison to the baseline scheme is quite small for $M = 16$, but it becomes relatively larger when M is increased from 16 to 36, suggesting

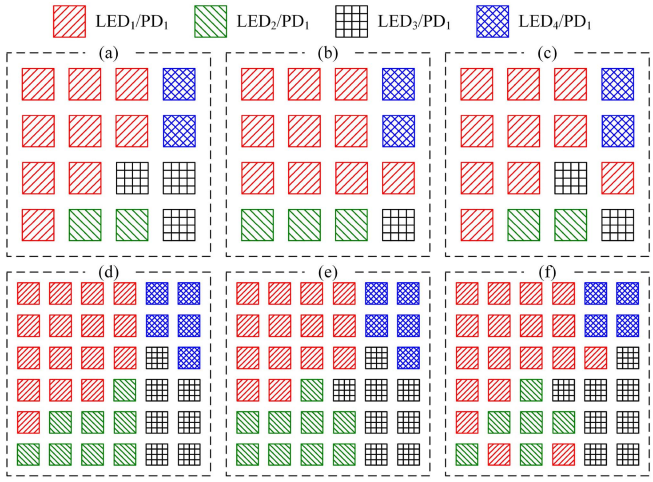

Fig. 10. Optimal IRS configuration for RC with (a) $M = 16$, position 1, 90 dB, (b) $M = 16$, position 2, 89 dB, (c) $M = 16$, position 3, 89 dB, (d) $M = 36$, position 1, 89 dB, (e) $M = 36$, position 2, 88 dB, and (f) $M = 36$, position 3, 87 dB.

that the use of IRS with optimal surface configuration is more beneficial when the IRS consists of more mirror units.

The BER versus transmitted SNR for the IRS-aided 4×4 MIMO-VLC system applying SM at different PD positions is plotted in Fig. 7. It can be observed that the optimal scheme can obtain relatively large SNR gains at all PD positions for both $M = 16$ and 36. Particularly, for $M = 16$, the optimal scheme outperforms the baseline scheme by SNR gains of approximately 2.2, 1.2, and 2.2 dB at position 1, position 2 and position 3, respectively. For $M = 36$, the optimal scheme achieves SNR gains of about 1.6, 1.2 and 1.3 dB at position 1, position 2 and position 3, respectively, when compared with the baseline scheme. Moreover, by increasing M from 16 to 36, SNR gains of 5.5, 6.2, and 5.5 dB can be attained by the optimal scheme at position 1, position 2 and position 3, respectively. Fig. 8 shows the BER versus transmitted SNR for the IRS-aided 4×4 MIMO-VLC system applying SMP at different PD positions. As can be seen, the optimal scheme can yield a much more significant SNR gain over the baseline scheme for SMP, when compared with RC and SM.

Fig. 9 depicts the achieved SNR gains according to the BER evaluations in Figs. 6–8. The SNR gains obtained by the optimal scheme over the baseline scheme at different PD positions for $M = 16$ and 36 are shown in Fig. 9(a) and (b), respectively. As we can see, the obtained SNR gains are not very significant for RC which hardly exceeds 1 dB. In contrast, much more significant SNR gains can be obtained by SM and SMP. Taking SMP and $M = 16$ as an example, the obtained SNR gains are 2.5, 3.8 and 2.4 dB at position 1, position 2 and position 3, respectively. The SNR gains obtained by the optimal scheme with $M = 36$ over that with $M = 16$ at different PD positions are shown in Fig. 9(c). Similarly, the SNR gains for RC with the optimal scheme are only about 1 to 2 dB, and meanwhile, the SNR gains for both SM and SMP with the optimal scheme can exceed 5 dB, with a maximum SNR gain achieved by SMP at position 2 reaching as high as 7.4 dB.

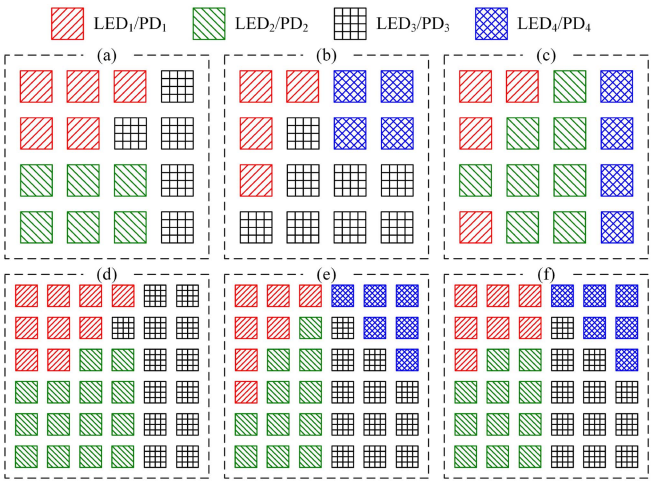

Fig. 11. Optimal IRS configuration for SM with (a) $M = 16$, position 1, 107 dB, (b) $M = 16$, position 2, 105 dB, (c) $M = 16$, position 3, 101 dB, (d) $M = 36$, position 1, 101 dB, (e) $M = 36$, position 2, 98 dB, and (f) $M = 36$, position 3, 95 dB.

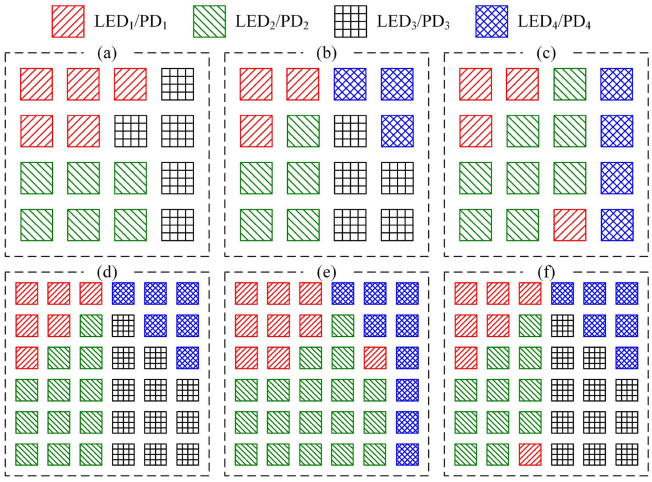

Fig. 12. Optimal IRS configuration for SMP with (a) $M = 16$, position 1, 115 dB, (b) $M = 16$, position 2, 112 dB, (c) $M = 16$, position 3, 109 dB, (d) $M = 36$, position 1, 109 dB, (e) $M = 36$, position 2, 105 dB, and (f) $M = 36$, position 3, 103 dB.

It can be concluded from Fig. 9 that the use of an IRS with optimal surface configuration can improve the performance of all three MIMO techniques in the considered 4×4 MIMO-VLC system.

C. Visualization of Optimal IRS Configurations

In this subsection, the visualization of various optimal IRS configurations is presented to clearly show how the surface of IRS is configured to achieve improved BER performance in the considered 4×4 MIMO-VLC system. Figs. 10, 11, and 12 depict the optimal IRS configurations for RC, SM and SMP with different M values, PD array positions and transmitted SNR values. As we can see, the optimal IRS configurations are generally different for different MIMO techniques with different system parameters. Moreover, for RC, as shown in Fig. 10, the optimal IRS configurations indicate that the IRS reflects all the signals from the four LEDs to PD_1. However, for SM and SMP, the optimal IRS configurations suggest that the IRS reflects the signals from the four LEDs to different PDs.

V. Conclusion

In this paper, we have investigated the optimization of IRS configuration in IRS-aided MIMO-VLC systems applying RC, SM and SMP, and a BER minimization problem has been formulated by employing the tight analytical BER upper bound. Since the problem is NP-hard in general, an optimization algorithm was proposed to decompose the original problem into three sub-problems, i.e., continuous relaxation and variable transformation, binary rounding, and feasible projection. The obtained simulation results demonstrate that the BER performance of an indoor IRS-aided 4×4 MIMO-VLC system can be greatly improved by adopting the optimal surface configuration scheme. More specifically, the SNR gain obtained by using the optimal surface configuration scheme in comparison to the baseline scheme is much more significant for SM and SMP. Therefore, IRS with optimal surface configuration can be a very promising candidate for substantial performance enhancement of MIMO-VLC systems.

References

[1] H. Haas, "Visible light communication," in *Proc. Opt. Fiber Commun. Conf.*, 2015, Paper Tu2G.5.
[2] N. Chi, Y. Zhou, Y. Wei, and F. Hu, "Visible light communication in 6G: Advances, challenges, and prospects," *IEEE Veh. Technol. Mag.*, vol. 15, no. 4, pp. 93–102, Dec. 2020.
[3] T. Komine and M. Nakagawa, "Fundamental analysis for visible-light communication system using LED lights," *IEEE Trans. Consum. Electron.*, vol. 50, no. 1, pp. 100–107, Feb. 2004.
[4] L. Zeng et al., "High data rate multiple input multiple output (MIMO) optical wireless communications using white LED lighting," *IEEE J. Sel. Areas Commun.*, vol. 27, no. 9, pp. 1654–1662, Dec. 2009.
[5] R. Mesleh, H. Elgala, and H. Haas, "Optical spatial modulation," *J. Opt. Commun. Netw.*, vol. 3, no. 3, pp. 234–244, Mar. 2011.
[6] T. Fath and H. Haas, "Performance comparison of MIMO techniques for optical wireless communications in indoor environments," *IEEE Trans. Commun.*, vol. 61, no. 2, pp. 733–742, Feb. 2013.
[7] A. Burton, H. Minh, Z. Ghassemlooy, E. Bentley, and C. Botella, "Experimental demonstration of 50-Mb/s visible light communications using 4× 4 MIMO," *IEEE Photon. Technol. Lett.*, vol. 26, no. 9, pp. 945–948, May 2014.
[8] J. Lian and M. Brandt-Pearce, "Multiuser MIMO indoor visible light communication system using spatial multiplexing," *J. Lightw. Technol.*, vol. 35, no. 23, pp. 5024–5033, Dec. 2017.
[9] C. Chen et al., "Enhanced OFDM-based optical spatial modulation," in *Proc. IEEE Int. Conf. Commun.*, 2021, pp. 1–6.
[10] A. Yesilkaya, E. Basar, F. Miramirkhani, E. Panayirci, M. Uysal, and H. Haas, "Optical MIMO-OFDM with generalized LED index modulation," *IEEE Trans. Commun.*, vol. 65, no. 8, pp. 3429–3441, Aug. 2017.
[11] C. Chen et al., "User-centric MIMO techniques for indoor visible light communication systems," *IEEE Syst. J.*, vol. 14, no. 3, pp. 3202–3213, Sep. 2020.
[12] C. Chen et al., "OFDM-based generalized optical MIMO," *J. Lightw. Technol.*, vol. 39, no. 19, pp. 6063–6075, Oct. 2021.
[13] T. Chen, L. Liu, B. Tu, Z. Zheng, and W. Hu, "High-spatial-diversity imaging receiver using fisheye lens for indoor MIMO VLCs," *IEEE Photon. Technol. Lett.*, vol. 26, no. 22, pp. 2260–2263, Nov. 2014.
[14] C. Chen, W.-D. Zhong, D. Wu, and Z. Ghassemlooy, "Wide-FOV and high-gain imaging angle diversity receiver for indoor SDM-VLC systems," *IEEE Photon. Technol. Lett.*, vol. 28, no. 19, pp. 2078–2081, Oct. 2016.

[15] A. K. Gupta and A. Chockalingam, "Performance of MIMO modulation schemes with imaging receivers in visible light communication," *J. Lightw. Technol.*, vol. 36, no. 10, pp. 1912–1927, May 2018.

[16] B. Qin, W. Wen, M. Liu, Y. Zhang, and C. Chen, "Indoor MIMO-VLC using angle diversity transmitters," *Sensors*, vol. 22, no. 14, Jul. 2022, Art. no. 5436.

[17] A. Nuwanpriya, S.-W. Ho, and C. S. Chen, "Indoor MIMO visible light communications: Novel angle diversity receivers for mobile users," *IEEE J. Sel. Areas Commun.*, vol. 33, no. 9, pp. 1780–1792, Sep. 2015.

[18] P. F. Mmbaga, J. Thompson, and H. Haas, "Performance analysis of indoor diffuse VLC MIMO channels using angular diversity detectors," *J. Lightw. Technol.*, vol. 34, no. 4, pp. 1254–1266, Feb. 2016.

[19] K. Ying, H. Qian, R. J. Baxley, and S. Yao, "Joint optimization of precoder and equalizer in MIMO VLC systems," *IEEE J. Sel. Areas Commun.*, vol. 33, no. 9, pp. 1949–1958, Sep. 2015.

[20] H. Yang, C. Chen, W.-D. Zhong, and A. Alphones, "Joint precoder and equalizer design for multi-user multi-cell MIMO VLC systems," *IEEE Trans. Veh. Technol.*, vol. 67, no. 12, pp. 11354–11364, Dec. 2018.

[21] C. Wang, Y. Yang, Z. Yang, C. Feng, J. Cheng, and C. Guo, "Joint SIC-based precoding and sub-connected architecture design for MIMO VLC systems," *IEEE Trans. Commun.*, vol. 71, no. 2, pp. 1044–1058, Feb. 2023.

[22] Q. Wu and R. Zhang, "Towards smart and reconfigurable environment: Intelligent reflecting surface aided wireless network," *IEEE Commun. Mag.*, vol. 58, no. 1, pp. 106–112, Jan. 2020.

[23] S. Aboagye, T. M. Ngatched, O. A. Dobre, and A. R. Ndjiongue, "Intelligent reflecting surface-aided indoor visible light communication systems," *IEEE Commun. Lett.*, vol. 25, no. 12, pp. 3913–3917, Dec. 2021.

[24] S. Sun, T. Wang, F. Yang, J. Song, and Z. Han, "Intelligent reflecting surface-aided visible light communications: Potentials and challenges," *IEEE Veh. Technol. Mag.*, vol. 17, no. 1, pp. 47–56, Mar. 2022.

[25] A. M. Abdelhady, A. K. S. Salem, O. Amin, B. Shihada, and M.-S. Alouini, "Visible light communications via intelligent reflecting surfaces: Metasurfaces vs mirror arrays," *IEEE Open J. Commun. Soc.*, vol. 2, pp. 1–20, 2021.

[26] A. M. Abdelhady, O. Amin, A. K. S. Salem, M.-S. Alouini, and B. Shihada, "Channel characterization of IRS-based visible light communication systems," *IEEE Trans. Commun.*, vol. 70, no. 3, pp. 1913–1926, Mar. 2022.

[27] S. Sun, F. Yang, and J. Song, "Sum rate maximization for intelligent reflecting surface-aided visible light communications," *IEEE Commun. Lett.*, vol. 25, no. 11, pp. 3619–3623, Nov. 2021.

[28] S. Sun, F. Yang, J. Song, and Z. Han, "Joint resource management for intelligent reflecting surface–aided visible light communications," *IEEE Trans. Wireless Commun.*, vol. 21, no. 8, pp. 6508–6522, Aug. 2022.

[29] L. Qian, X. Chi, L. Zhao, and A. Chaaban, "Secure visible light communications via intelligent reflecting surfaces," in *Proc. IEEE Int. Conf. Commun.*, 2021, pp. 1–6.

[30] S. Sun, F. Yang, J. Song, and Z. Han, "Optimization on multiuser physical layer security of intelligent reflecting surface-aided VLC," *IEEE Wireless Commun. Lett.*, vol. 11, no. 7, pp. 1344–1348, Jul. 2022.

[31] Q. Wu, J. Zhang, Y. Zhang, G. Xin, and J. Guo, "Configuring reconfigurable intelligent surface for parallel MIMO visible light communications with asymptotic capacity maximization," *Appl. Sci.*, vol. 13, no. 1, Dec. 2022, Art. no. 563.

[32] S. Sun, W. Mei, F. Yang, N. An, J. Song, and R. Zhang, "Optical intelligent reflecting surface assisted MIMO VLC: Channel modeling and capacity characterization," *IEEE Trans. Wireless Commun.*, vol. 23, no. 3, pp. 2125–2139, Mar. 2024.

[33] S. Sun, F. Yang, J. Song, and R. Zhang, "Intelligent reflecting surface for MIMO VLC: Joint design of surface configuration and transceiver signal processing," *IEEE Trans. Wireless Commun.*, vol. 22, no. 9, pp. 5785–5799, Sep. 2023.

[34] R. K. Pal, S. P. Dash, S. Aïssa, and D. Ghose, "Outage probability analysis of RIS-assisted indoor wide-fOV-VLC/RF wireless communication," *IEEE Wireless Commun. Lett.*, vol. 13, no. 1, pp. 34–38, Jan. 2024.

[35] B. G. Guzman, M. M. Cespedes, V. P. G. Jimenez, A. G. Armada, and M. Brandt-Pearce, "Resource allocation exploiting reflective surfaces to minimize the outage probability in VLC," 2024, *arXiv:2401.16627*.

[36] P. Chvojka, S. Zvanovec, P. Haigh, and Z. Ghassemlooy, "Channel characteristics of visible light communications within dynamic indoor environment," *J. Lightw. Technol.*, vol. 33, no. 9, pp. 1719–1725, May 2015.

[37] S. Aboagye, A. R. Ndjiongue, T. M. Ngatched, O. A. Dobre, and H. V. Poor, "RIS-assisted visible light communication systems: A tutorial," *IEEE Commun. Surveys Tut.*, vol. 25, no. 1, pp. 251–288, Firstquarter 2023.

[38] X. Guo and N. Chi, "Superposed 32QAM constellation design for 2×2 spatial multiplexing MIMO VLC systems," *J. Lightw. Technol.*, vol. 38, no. 7, pp. 1702–1711, Apr. 2020.

[39] J. G. Proakis and M. Salehi, *Digital Communi*. New York, NY, USA: McGraw-Hill, 2008.

[40] A. Stavridis and H. Haas, "Performance evaluation of space modulation techniques in VLC systems," in *Proc. IEEE Int. Conf. Commun. Workshops*, 2015, pp. 1356–1361.

[41] M. Chiani, D. Dardari, and M. K. Simon, "New exponential bounds and approximations for the computation of error probability in fading channels," *IEEE Trans. Wireless Commun.*, vol. 2, no. 4, pp. 840–845, Jul. 2003.

[42] S. P. Boyd and L. Vandenberghe, *Convex Optimization*. Cambridge, U.K.: Cambridge Univ. Press, Mar. 2004.

[43] R. Meyer, "A class of nonlinear integer programs solvable by a single linear program," *SIAM J. Control Optim.*, vol. 15, no. 6, pp. 935–946, Nov. 1977.

[44] W. Wen, Z. Chen, H. H. Yang, W. Xia, and T. Q. Quek, "Joint scheduling and resource allocation for hierarchical federated edge learning," *IEEE Trans. Wireless Commun.*, vol. 21, no. 8, pp. 5857–5872, Aug. 2022.

[45] A. Ben-Tal and A. Nemirovski, *Lectures on Modern Convex Optimization: Analysis, Algorithms, and Engineering Applications*. Philadelphia, PA, USA: SIAM, Jan. 2001.